JOURNAL OF OPTOELECTRONICS AND ADVANCED MATERIALS Vol. 9, No. 6, June 2007, p. 1918 - 1925

Algorithm for angular correction of images in scanning LIF

J. STRIBER, F. COLAO[a], R. FANTONI[a], L. FIORANI[a*], A. PALUCCI[a]
CERTO-INOE, Bucarest Romania
[a]ENEA, FIM-FISLAS, Via Enrico Fermi 45, Frascati, Italy

This paper deals with the angular dependence of laser backscattered and fluorescence signals from real target which are scanned in order to determine the actual preservation status of the surface by means of the laser induced fluorescence technique. Different correction algorithms have been proposed and tested on targets with a different fraction lambertian behavior (homogeneous scatterers). The results have been applied in scanning the real surface of a painted icon, for which a RGB image has been reconstructed from the separate fluorescence images collected and processed.

(Received November 17, 2006; accepted April 26, 2007)

Keywords: Laser induced fluorescence, Lidar fluorosensor, Cultural heritage

1. Introduction

Nowadays, the conservation and preservation of our cultural heritage is of main concerns, particularly in Europe [1-2]. The increasing need for non-destructive investigation tools has become a major issue [3-4], as sampling is in most cases restricted in view of the value or the uniqueness of the object. Artworks as wall paintings in buildings and monuments of historical interest are affected by environment (temperature and humidity) and human (pollutant releases) impact and therefore modified over time [5-7].

An apparatus measuring the laser induced fluorescence (LIF) has been built at ENEA Frascati, for application to artwork conservation and environmental monitoring.

LIF measurement relies on the information carried by two different channels: spectral position and spectral intensity. Generally speaking the first can be associated to the presence of specific fluorofores in the sample under study, while the second can be related to the amount of pigments. Unfortunately, it is known that intensity of reflectance and fluorescence may have an angular dependence. The ideal lambertian case of uniform intensity at different angles is rarely found in practice, and the recovery of the signal from the case of a perfectly flat surface to the real one is essential to increase measurement accuracy.

The purpose of this experiment was to measure the angular dependence of LIF in different samples, and to derive suitable data analysis algorithms and techniques by using reflectance and fluorescence data to make angular corrections.

2. Experimental apparatus

The scanning lidar fluorosensor experimental apparatus was designed by keeping in mind that very often artworks and specially fresco's on tombs are placed in small chambers with narrow entrances, where only a limited space can be used. In order to facilitate field operations the optical and mechanical supports have been assembled in a box, with a low weight and transportable. In the present set up the apparatus was optimized to monitor remote targets for working distances up to 10m maximum, its main characteristics are summarized in Table 1.

The light source is a compact pulsed, diode pumped, solid state laser, emitting in the UV either at @ 355 nm or at 266 nm, a residual emission at 532nm is also present into the outcoming beam. A set of optics (mirrors, lens and quartz fiber optic) allow to transmit the exciting radiation and to receive the scattering and fluorescence signals from the investigated target. A coaxial transmitter/receiver schema (see Fig. 1) was obtained by using a holed mirror (3 mm hole diameter in mirror M_1) crossed by the laser beam before reflection on the scanning mirror (M_2) used also for collecting the radiation emitted by he sample.

Optical surfaces were machined in ENEA Frascati laboratories, where a facility for polishing spherical optics on different bulk materials like aluminum, copper, fused silica glass and quartz is available. For LIF measurements an aluminum-zinc alloy has been used (Al-Zn ERGAL), because it gives high mechanical stability and robustness, while assuring a nearly constant reflection coefficient in the entire nearUV - visible spectrum from 350 to 800nm. Another important aspect to be considered in the material choice is the threshold for damage, also related to the resistance to the presence of dust, which is higher in uncoated metal mirrors with respect to more conventional dielectric mirrors. In particular the possibility of field use of the current experimental apparatus relies on this

property because the laser beam is directly reflected onto the last metallic steering mirror beafore reaching the target.

The last mirror M_2 is actuated by a two rotating servo controls operating at high accuracy. The M_2 mirror is capable to rotate along two orthogonal axes, thus allowing for a theoretical scan of an 2π sr, however the practical aperture of the scanning is limited by the mounting assembly reducing it to approximately +/- 45° deg in both horizontal and vertical axis. Rotary actuators are DC type with high accuracy both in positioning and repeatability.

Table 1. LIF main characteristics.

Laser	Thomson DIVA	Nd:YAG III Harmonic	Diode pumped	λ = 355 nm
			Energy per pulse	6 mJ @ 20 Hz
			Pulse length	10 ns
			Repetition rate	20 Hz
Spectrometer	Ocean Optics	S2000	CCD linear array	2048 elements silicon
			Detector spectral range	200 – 1100 nm
			Sensitivity	86 photons/count
		Fiber Optic	SMA 905	Single strand 0.22 NA
			Integration Time	8 ms
Optics		PP Mirrors N° 3	ERGAL Aluminum	15 cm diameter
		BK7 Lens	3" inch diameter.	f = 15 cm
Actuators	NRC	N° 2	Model 495-A, rotary stage	
			Travel range	360° continuous
	Resolution	0.001°	Min. Increment. Motion	0.003°

The fluorescence and backscattered radiation is optically driven by mirrors M_1 and M_3 through a BK7 collecting lens (L) and focused at the entrance of a fiber optic (F/O fused silica, 1 m long) linked to a compact spectrometer (S2000 OceanOptics ^{TM}). The CCD detector in the spectrometer permits to record the overall spectral emission with 1 nm resolution in the range between 200 up to 900 nm. Data are transferred to a PC Notebook via a dedicated LabView 6.0 software interface which also defines the instrument settings and data acquisition. The system was conceived to give information about a limited number of spectral bands, but the high resolution spectrometer used and the availability of the full fluorescence spectrum can extend the operational capability of the instrument from multispectral to hyperspectral. In the latter operation mode it is possible to acquire as many as 70 contiguous spectral bands with a resolution of 10 nm and a spectral range form 200 to 900 nm. For the present measurements only eight spectral bands were acquired.

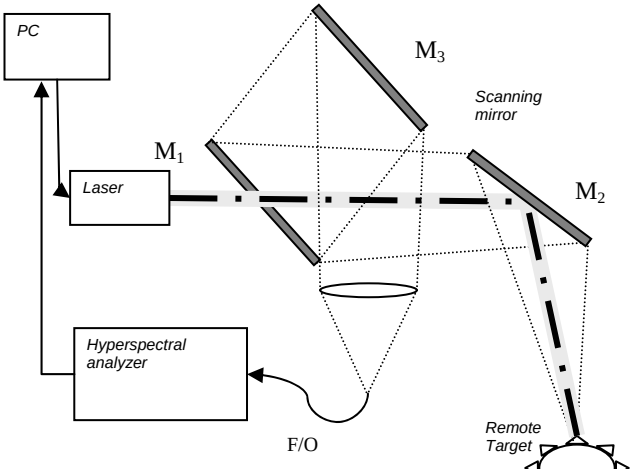

Fig. 1. Experimental set-up used for the present measurements.

3. Geometry of the receiver

Our purpose was to collect signal from a flat target upon which a laser beam was incident with an angle in the range $[-\pi, \pi]$. Two possibilities are given:

1. Keep fix everything but the angular position of the sample
2. Make the LIF scanning onto a cylindrical target in a direction orthogonal to the cylinder axis.

While the first possibility assures the complete independence on experimental parameter (like source-target distance), the second has been selected, because it is the actual configuration we use on field, and because it was easier to implement. To have conditions depending on the angular position only two conditions must be satisfied:

3. The cylinder radius r must be much greater than the laser footprint h; i.e. $r >> h$;
4. Source – target distance d must be much greater than cylinder radius r; i.e. $r << d$.

The geometry of the experimental apparatus is sketched in Fig. 2.

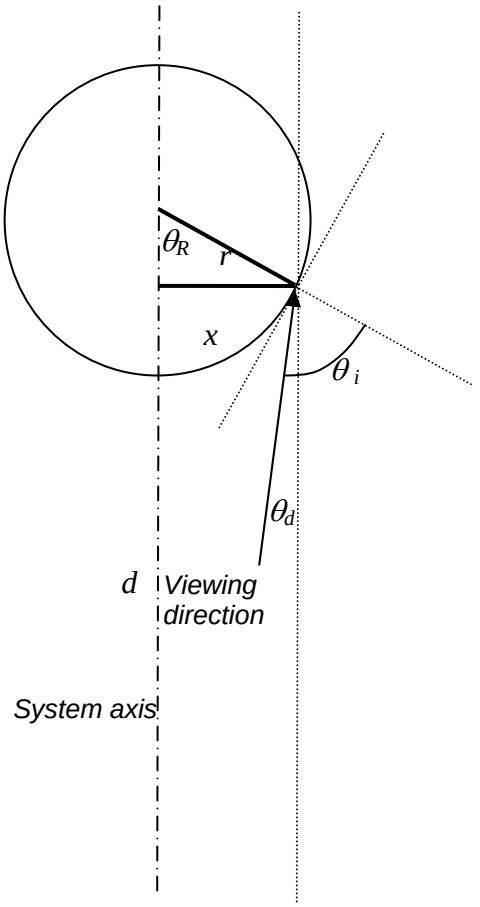

Fig. 2. Geometry of the experimental apparatus.

By inspection of Fig. 2, we get the relation between incidence angle θ_i , scanning angle θ_d and the angle at the cylinder center θ_R

$$\theta_i = \theta_R + \theta_d \quad (1)$$

After few simple trigonometric derivations, it results

$$x = r \sin \theta_R \quad (2)$$

$$x = (d + r\,(1-\cos \theta_R))\ \mathrm{tg}\ \theta_d \quad (3)$$

By combining eq. (2) and (3), we obtain

$$\sin \theta_R = (d / \mathrm{r} + 1-\cos \theta_R)\ \mathrm{tg}\ \theta_d \quad (4)$$

which, after simple algebra, reduces to

$$\sin (\theta_R + \theta_d) = (d / \mathrm{r} + 1) \sin \theta_d \quad (5)$$

Eq. (5) gives us θ_R which is inserted into eq. (1) to get the relation between scanning angle θ_i and the incident angle θ_d. Then we have to relate the pixel number i to incidence angle, this is done by considering that while scanning an image, the angular step $\delta\theta_s$ between adjacent points (giving the corresponding pixel) is kept constant. Let us indicate as:

- i a generic pixel number
- i_{start} and i_{stop} respectively the first and the last pixel corresponding to that angular position at which the laser beam hits the target
- $\delta\theta_s$ the angular step $\delta\theta_s = \dfrac{2\ \sin^{-1} \dfrac{r}{r+d}}{i_{stop} - i_{start}}$

then we have:

$$\theta_d = [\, i - (\, i_{\mathrm{start}} + i_{\mathrm{stop}})/2] \ \delta\theta_s \quad (6)$$

and finally the relationship between the pixel number and the angle of incidence:

$$\theta_i = \sin^{-1}\{ (d / \mathrm{r} + 1) \sin [\, i - (\, i_{\mathrm{start}} + i_{\mathrm{stop}})/2] \ \delta\theta_s\} \quad (7)$$

In Fig. 3 the angle of incidence as function of pixel number is reported. For the present case the cylinder diameter was 175 mm, working distance 1780 mm, pixels' values at which the laser beam is tangent to the cylinder are 14.0 and 90.6 (computed by interpolation).

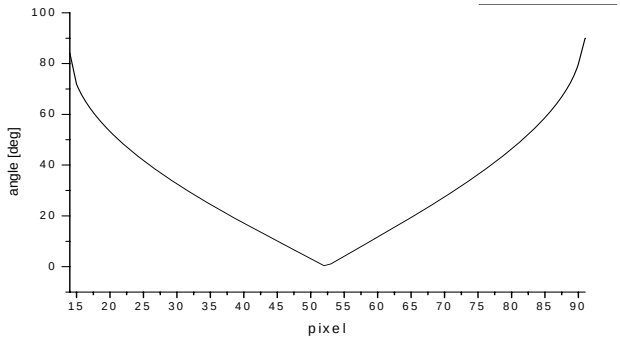

Fig. 3. Incidence angle as function of pixel number.

4. Lambertian target

White paper (Laser and Inkjet printer quality) was used as first sample. This material was selected because it has a little surface roughness, it is highly fluorescent when excited in the UV and can be assumed as a standard target. The exciting laser radiation was set at 266nm and signal was acquired at the spectral positions corresponding to relative maxima in the fluorescence spectrum. In the case of white paper the observed spectral bands were 425 nm, 440 nm, 475 nm each of them acquired with 10 nm spectral width. A channel for elastic scattering (reflectance) was also added at 532 nm. Reflectance on the laser second harmonic N_{532} was obtained by subtracting the florescence tail evaluated as an average of two adjacent channels at 522 nm and 542 nm (named respectively F_{522} and F_{542}), according to the following relation:

$$N_{532} = F_{532} - (F_{542} + F_{522}) / 2 \quad (8)$$

The source – target distance was 1780 mm, and the cylinder diameter was 175 mm.

The fist image was a cylinder: scanned area was 100 pixels, 5 rows were acquired for statistical purpose. Results are shown in Fig. 4 where the relative intensity on the acquired fluorescence bands (averaged on 5 rows) are plotted as function of incidence angle.

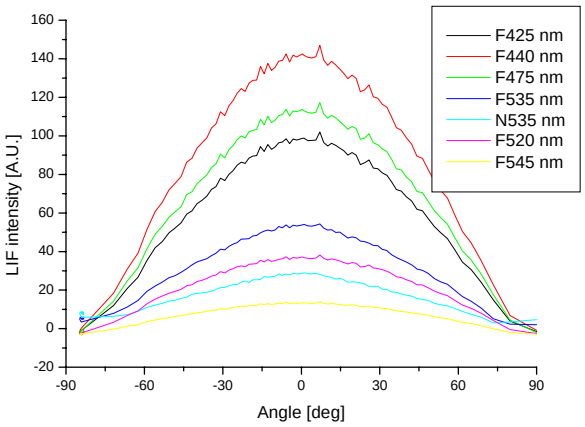

Fig. 4. Raw signal intensity for 8 bands as function of the incidence angle. Target: white paper, distance 1780 mm.

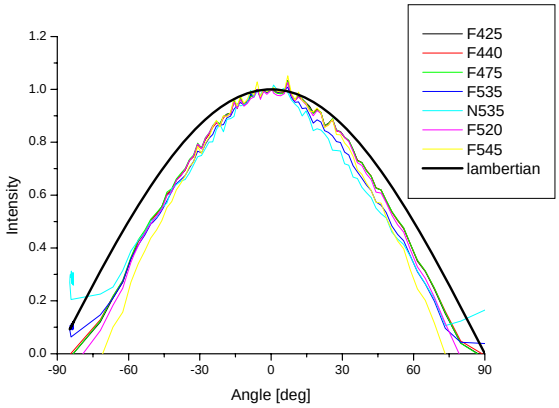

Fig. 5. Normalized signal intensity for 8 bands as function of the incidence angle. Black bolded line is relative to an ideal lambertian surface having an angular emission as cos θ.

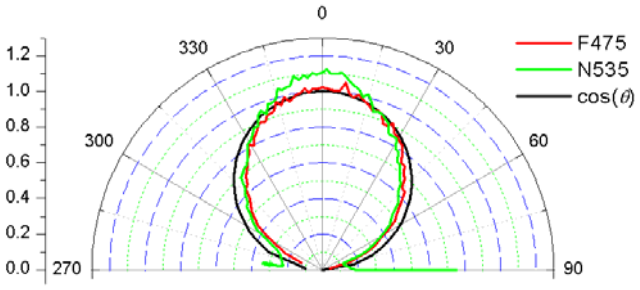

Fig. 6. Polar plot of three selected channel of figure 5: normalized and corrected elastic channel at N_{532} ,(green line), normalized to maximum fluorescence at F_{475} (red line), ideal lambertian surface (black line).

The examination of Fig. 6 reveals a close resemblance of the angular dependence between the reflectance signal at 532 nm and the fluorescence at 475 nm, unfortunately neither the first nor the second follows the cosine emission law typical of an ideal scattering surface. In both the analyzed cases the emission at small angles (lower than 15 deg) is close to the ideal case, while at larger angles a significant deviation starts to appear.

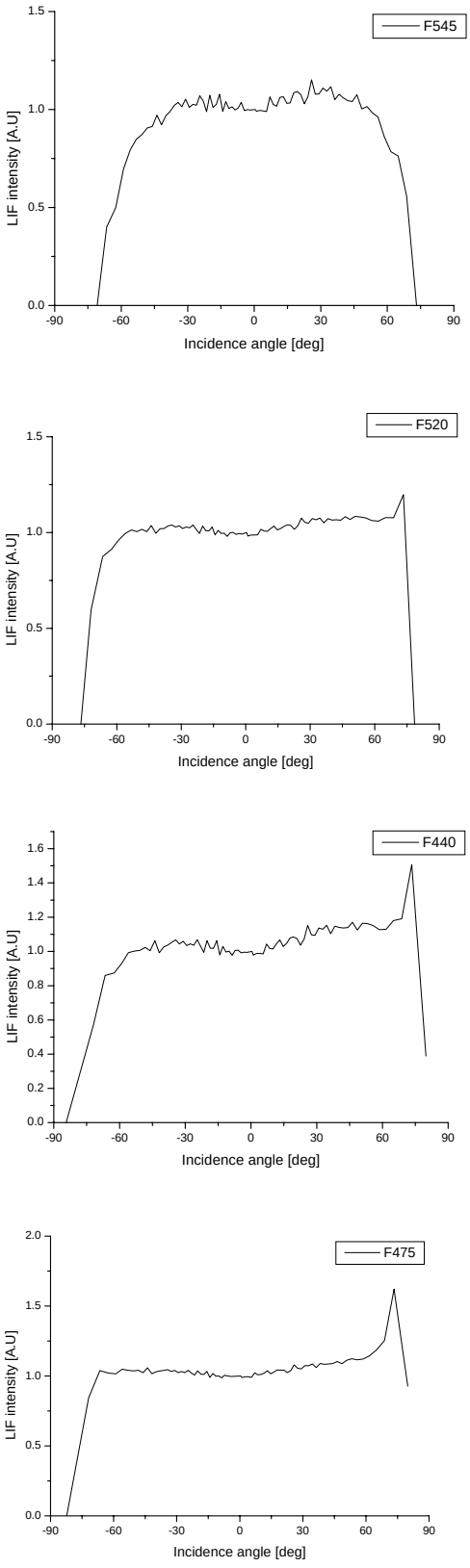

Fig. 7. Result of the correction for the incidence angle eq. (9) applied to data of Fig. 5.

The similar angular dependence experimentally observed in the elastic channel and in the fluorescence could be used for correction on target with known spectral properties, as in the present case where it is sure that the spectral characteristic of the investigated area in different angular position is not changing.

The algorithm proposed for angular correction is to normalize the florescence channel to the elastic one, according the following equation:

$$N_f = \frac{F_f - B_f}{F_{532} - B_{532}} \tag{9}$$

where N_f is the normalized fluorescent channel,

F_f and B_f are respectively the raw fluorescent channel and its background,

F_{532} and B_{532} are respectively the raw reflectance channel and its background.

If we apply eq. (9) to the data reported in Fig. 5, we obtain the result shown in Fig. 7.

We expect that the effect of the angular correction is to remove the changes in signal intensity due to the incidence angle, and the advantage is a dramatic increase of the linearity of the response, as reported in Fig. 7. Here we note in fact that the amplitude of the signal remains constant within of +/- 10% and in an angular range of more than 120 deg, thus confirming for this specific surface the beneficial effect of normalization on the elastic channel.

This result is encouraging, however less favourable cases must also be considered. Surfaces showing considerable reflection, or in general surfaces composed by a great number of randomly orientated small reflecting fragments (i.e. gold varnish on wood paintings) belong to this category.

In order to test a surface with a high reflectance we used a plastic sheet loaded with a fluorescent dye, in the following referred as “yellow target”. By repeating the measure as in the case of white paper we get the result shown in Fig. 8.

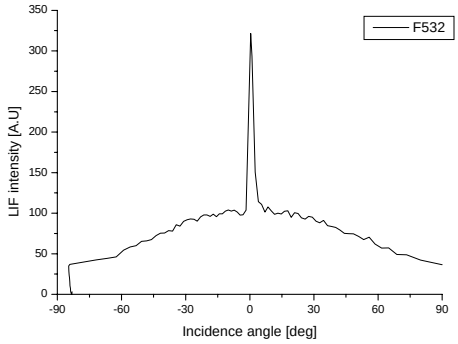

Fig. 8. Relative signal intensity for elastic channel at 532 nm as a function of the incidence angle, on a partially reflecting yellow target.

In this case the angular response is dominated by the very strong contribution near an angle at 0 deg where we expect to be close to the position of specular reflection. We note that the correction of eq. (9) can still be applied, but it is effective only on angles not too close to the position of reflection (in this case > 5 deg), while it must not be applied in the angular range of +/- 5deg, where its effect is to overcorrect the fluorescence signal.

We conclude first that an angular correction for LIF signal intensity due to the incidence angle can be made by using the elastic channel at 532nm, although this correction is safe only on targets which are known to have a very low specular reflection.

To properly estimate the reflectance at 532 nm the method of adjacent band subtraction has been demonstrated to be an effective one, and for the present measurements it has been thoroughly applied.

5. Sample scan on wood icon

As a test for the correction algorithm suggested in the former section, a LIF scan has been performed on the wood icon shown in Fig. 9.

Fig. 9. Picture of the wood icon used to test correction algorithms.

5.1. Background subtraction

To take into account for the fluorescence tail which can affect the signal intensity on a given fluorescence or reflectance channel, the following simple subtractive algorithm is proposed:

$$N_f = F_f - \frac{B_{f1} + B_{f2}}{2} \tag{10}$$

were the background bands B_{f1} and B_{f2} are the adjacent bands as near as possible to the considered channel. The proposed algorithm gives correction in case of non flat background fluorescence, i.e. when the channel to be corrected is located on or near the shoulder of a strong fluorescence emission. It the cases when only one adjacent channel is given. Eq. (10) can still be applied if we make the assumption $B_{f1} = B_{f2}$.

In Fig. 10 we report the raw data signal intensity of F532 channel, together with those of channels F522 and F542, in abscissa it is shown the pixel number in the range 1000-1400 corresponding to approximately 2 scanned

lines. Band at F532 is higher than the two adjacent bands, namely at F522 and F542, which appear to be very similar.

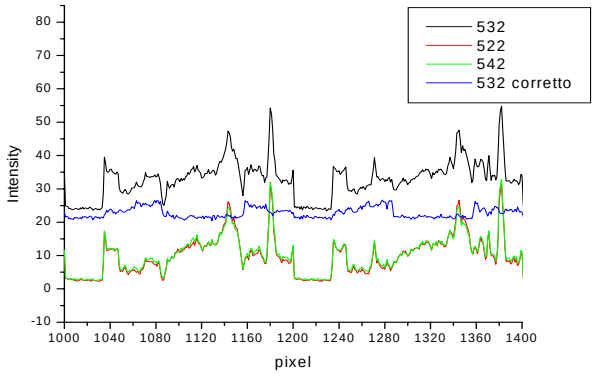

Fig. 10. Background correction for elastic channel F532 (nominal position: 532 nm, width: 10 nm).

After the background correction we notice that the signal at F532 is only weakly modulated but still partially correlated to the adjacent spectral bands. Main changes in the F532 can now be related to changes in reflectance from pigment on the target.

The residual correlation seems to indicate that the normalization to F532 can in some case decrease the image contrast.

5.2. LIF scans

Scan of the icon shown in Fig. 9 have been acquired at the spectral position reported in Table 2.

Table 2. Spectral position and width for multispectral acquisition of icon.

Channel #	Acquisition channel	Band center	Bandwidth	Notes
1	3	355	10	Reflectance at THG
2	4	446	10	See Fig. 11e
3	5	460	10	
4	6	490	10	
5	7	522	10	See Fig. 11d
6	8	532	10	Reflectance at SHG Fig. 11a
7	9	542	10	See Fig. 11f
8	10	630	10	See Fig. 11c
9	11	640	10	
10	12	660	10	
11	13	750	10	
12	14	550	350	Total fluorescence Fig. 11b

All the images shown in Figs. 11a – 11f are corrected by using eq(10): in this case the background channel was F750 (nominal position: 750 nm, width: 10 nm). By examination of Fig. 11 we note that the fluorescence on red channel has more details than other bands, this could possibly be related to the brownish dominant color of the icon.

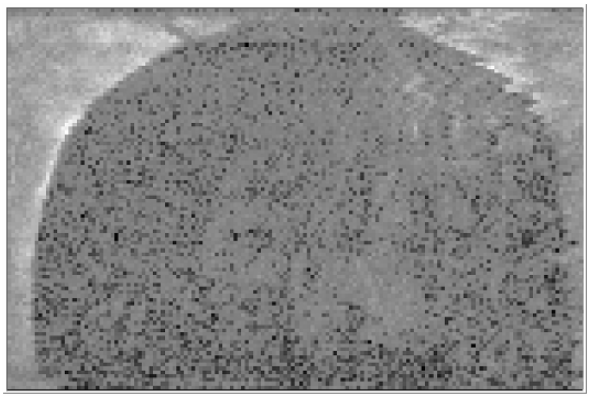

Fig. 11a. Wood icon. Image size: 200 x 100 pixel, channel: 532 nm, FWHM: 10 nm, algorithm: background corrected.

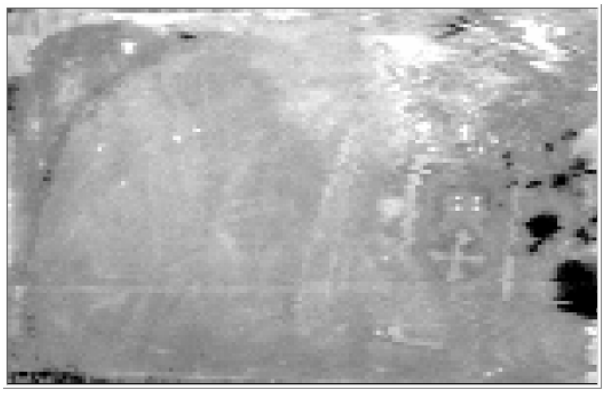

Fig. 11b. Wood icon. Image size: 200 x 100 pixel, channel: 550 nm, FWHM:150 nm algorithm: background corrected.

Fig. 11c. Wood icon. Image size: 200 x 100 pixel, channel: 630 nm, FWHM: 10 nm, algorithm: background corrected.

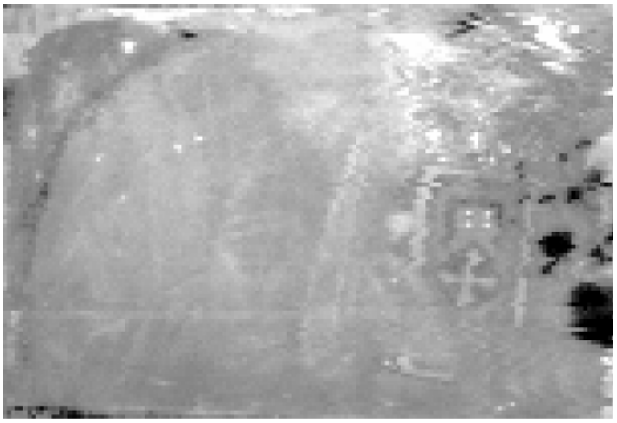

Fig. 11d. Wood icon. Image size: 200 x 100 pixel, channel: 522nm, FWHM: 10nm, algorithm: background corrected.

Fig. 11e. Wood icon. Image size: 200 x 100 pixel, channel: 446 nm, FWHM: 10nm, algorithm: background corrected.

Fig. 11f. Wood icon. Image size: 200 x 100 pixel, channel: 542 nm, FWHM: 10 nm, algorithm: eq.(10).

Fig. 12 shows RGB colored image obtained by combining R:F630, G:F522, B:F446 channel. Algorithm of eq.(10) was applied to each channel. The meaning of intense spots is actually not clear: it might be related to areas of bad preservation.

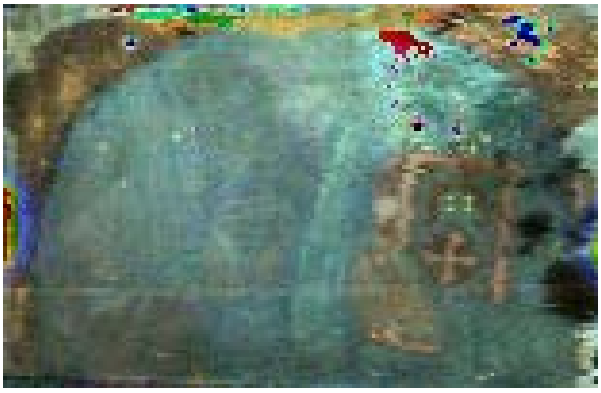

Fig. 12. Wood icon: RGB colored image obtained by combining R:F630, G:F522, B:F446 channels.

Due to a correlation still present between the channel N532 and the adjacent fluorescence channels (see Fig. 10), and due to the fact that in case of wood icon the surface is approximately flat, we expect the algorithm of eq.(9) could not really improve the image enhancing further details.

The intensity of the channel at 532 nm (elastic channel) taken at row 10 of the image is reported in Fig. 13. It is possible to notice that the target reflectance has two different levels having approximately a constant value. The first level appearing to the right part of the graph, has higher signal intensity and could be related to a gold layer. A second level starting from pixel # 50 has a lower value still constant.

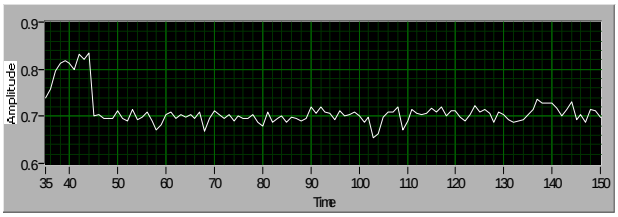

Fig. 13. Intensity of F532 channel at pixel row 10.

6. Conclusion

Results obained on the icon are quite encouraging for the application of the diagnostic to cultural heritage preservation when dealing with painted surfaces, even if their behavoiur is by far non lambertian, provided that mirror reflection conditions are avoided during the scanning.

However the correlation still present between elastic channel and fluorescence suggests a refinement of the correction algorithm, i.e. normalization could be made using the N532 channel at which is subtracted the part correlated with the total fluorescence image.

Acknowledgments

This work was funded by TECSIS project, ENEA RES office is gratefully acknowledged for supporting the grant to J. Striber. The authors want to express their gratitude to the P. Aristipini, D. Del Bugaro, R. Giovagnoli and G. Terranova for their valuable assistance during the present work.

References

[1] R. Mitchell, Environmental Science & Tecnology, March, **34**(5), 105 A (2000).
[2] V. Cappellini, Maitre; Pitas; Piva; IEEE Transactions, **13**(3) , March 273 – 276 (2004).
[3] J. F. Asmus, J. Cultural Heritage **4**, 289-293, (2003).
[4] V. Zafiropulos, C. Fotakis. "Lasers in the conservation of painted artworks" Chapter 6 in Laser Cleaninig in Conservation: An Introduction, ed. M. Cooper (Butterworth Heinemann Oxford), 79-90 (1998).
[5] A. Sgamellotti, Journal of Cultural Heritage **4**, 303s-308s (2003).
[6] P. Weibring, T. Johansson, H. Edner, S. Svanberg, B. Sundnér, V. Raimondi, G. Cecchi, L. Pantani, Applied Optics **40**, 6111-6120 (2001).
[7] R. Fantoni, A. Palucci, S. Ribezzo, I. Borgia, E. Bacchi, M. Caponero, A. Bordone, L. Businaro, M. Ferri De Collibus, G. Fornetti, C. Poggi, "Laser diagnostics for conservation and restoration of cultural inheritance", SPIE Proc. ALT99, V. I. Pustovoy, V. I. Konov, eds., Bellingham, Washington, vol. **4070**, 2-7, (2000).

*Corresponding author: fiorani@frascati.enea.it

Appendix A

A computer code was used to solve the eq. (7) in the text. A table is given, reporting the angle of incidence as function of pixel number for the present measurement.

Table A1. Angle of incidence as function of the pixel number in the experiment having a cylinder od diameter 175 mm, working distance 1780 mm. Pixels' values at which the laser beam is tangent to the cylinder are 14 and 90.6 (computed by interpolation).

0	83.00		30	32.63		60	11.60
1	83.14		31	30.95		61	13.13
2	83.27		32	29.30		62	14.68
3	83.40		33	27.69		63	16.23
4	83.54		34	26.10		64	17.79
5	83.67		35	24.55		65	19.37
6	83.81		36	23.01		66	20.97
7	83.94		37	21.51		67	22.58
8	84.07		38	20.02		68	24.21
9	84.21		39	18.55		69	25.86
10	84.34		40	17.09		70	27.53
11	84.47		41	15.65		71	29.23
12	84.61		42	14.23		72	30.96
13	84.74		43	12.81		73	32.72
14	84.18		44	11.41		74	34.52
15	71.89		45	10.01		75	36.36
16	66.55		46	8.63		76	38.24
17	62.46		47	7.25		77	40.17
18	59.00		48	5.87		78	42.16
19	55.95		49	4.50		79	44.21
20	53.18		50	3.14		80	46.33
21	50.63		51	1.77		81	48.54
22	48.25		52	0.41		82	50.86
23	46.00		53	1.05		83	53.29
24	43.86		54	2.54		84	55.87
25	41.82		55	4.04		85	58.63
26	39.86		56	5.55		86	61.64
27	37.97		57	7.05		87	64.97
28	36.14		58	8.56		88	68.77
29	34.36		59	10.08		89	73.39